Dual Circularly-Polarized Broadside Beam Metasurface Antenna

A. Tellechea, F. Caminita, E. Martini, *Senior Member, IEEE*, I. Ederra, *Member, IEEE* ,J.C. Iriarte, R.Gonzalo, *Member, IEEE,* S. Maci, *Fellow, IEEE*

***Abstract*— This paper presents the design of a modulated metasurface (MTS) antenna capable to provide both right-hand (RH) and left-hand (LH) circularly polarized (CP) boresight radiation at Ku-band (13.5GHz). This antenna is based on the interaction of two cylindrical-wavefront surface wave (SW) modes of TE and TM types with a rotationally symmetric, anisotropic modulated MTS placed on top of a grounded slab. A properly designed centered circular waveguide-feed excites the two orthogonal (decoupled) SW modes and guarantees the balance of the power associated with each of them. By a proper selection of the anisotropy and modulation of the MTS pattern, the phase velocities of the two modes are synchronized and leakage is generated in broadside direction with two orthogonal linear polarizations. When the circular waveguide is excited with two mutually orthogonal TE_{11} modes in phase-quadrature, an LHCP or RHCP antenna is obtained. This paper explains the feeding system and the MTS requirements that guarantee balanced conditions of the TM/TE SWs and consequent generation of dual circularly polarized boresight radiation.**

***Index Terms*— Antennas, metasurfaces, surface waves, leaky waves, surface impedance , dual polarization, RHCP, LHCP.[1]**

I. Introduction

In the last years, modulated metasurface (MTS) antennas have been proposed as innovative, thin, low mass alternative to conventional bulky configurations for satellite applications requiring medium-to-large gain antennas [1]-[8]. MTS antennas are constituted by metallic patches printed on a grounded slab, and therefore, they are realized through consolidated and low cost technologies.

The first realization of the MTS antenna concept was presented five years ago, with the development of holographic antennas. In [1], for the first time, pencil beam-shaped radiation was obtained by properly shaping the isotropic (scalar) or anisotropic (tensor) surface impedance of a MTS. A leaky wave antenna with sinusoidally-modulated surface reactance was manufactured in [2]. A circularly polarized broadside beam antenna based on the interaction between a cylindrical surface wave (SW) launched from a centered point feed and anisotropic surface impedance with a spiral-shaped modulation is presented in [3]. As shown in [4],[5], when the spiral-shaped modulation is accompanied by a proper anisotropy of the surface impedance, the cross-polarization level can be drastically reduced. The flexibility and the simplicity of this technology in designing different shapes of radiation diagrams is extraordinarily attractive, especially for different satellite applications in which pencil beams or isoflux radiation patterns are needed [6]-[8]. In some systems, several MTSs are employed in order to improve the overall antenna performance. This is the case for instance in [9], where two different MTSs have been combined to obtain a high-gain low profile lens antenna and in [4], where two separate MTSs have been employed to obtain dual-pol broadside beam radiation.

Nowadays, the capability to provide dual-circular polarization with a unique MTS aperture is still a challenge. This paper, for the first time, presents a MTS antenna capable to provide both right-hand circular polarization (RHCP) and left-hand circular polarization (LHCP) in boresight direction at 13.5GHz.

Two simultaneous SWs are launched by the same feed, characterized as transverse electric (TE) and transverse magnetic (TM) modes. These modes are matched in phase and balanced in amplitude. Phase matching is ensured by selecting an appropriate anisotropic MTS, which allows for almost independent control of the phase velocities of the two modes, due to their polarization decoupling. However, amplitude balance is provided by a proper design of the feeding structure.

The paper is structured as follows. Section II presents the basic operation principle of the configuration, analyzing the balanced-impedance boundary conditions. In Section III, the required characteristics of the surface impedance modulation are studied. Section IV describes in detail the feeding system necessary to obtain dual polarization behavior. Section V shows the design and implementation of an ideal metasurface, which has been designed based on the previous theoretical analysis, including the details of the subwavelength pixel-

This work was supported by COST ACTION IC1102, NEWFOCUS Research Networking Program and Spanish Ministry of Science and Innovation (project TEC2013-47753-C3-1-R).

A. Tellechea, I. Ederra, J.C. Iriarte and R. Gonzalo are with the Antenna Group, Department of Electrical and Electronic Engineering, Public University of Navarra, 31006 Navarra, Spain (e-mail: amagoia.tellechea@unavarra.es; inigo.ederra@unavarra.es; jcarlos.iriarte@unavarra.es; ramon@unavarra.es).

F.Caminita and E. Martini are with the Department of Information Engineering and Mathematics, University of Siena, 53100 Siena, Italy and with Wave Up Srl, 50126 Firenze, Italy (e-mail: caminita@dii.unisi.it; martini@dii.unisi.it).

S. Maci is with the Department of Information Engineering and Mathematics, University of Siena, 53100 Siena, Italy (e-mail: macis@dii.unisi.it).

Digital Object Identifier XXXXXXXXXXXXXXX

elements required to synthesize the MTS configuration, and the relevant full-wave simulation. Conclusions are drawn in Section VI.

II. Basic Operation Principle

This antenna operates on the excitation of two cylindrical SWs characterized as TE_z and TM_z modes, where z is the normal to the surface. These modes are decoupled in power and possess similar dispersion diagrams in a certain frequency band; namely, in that frequency range they propagate with approximately the same phase velocity. Furthermore, by employing an appropriate feed, their amplitudes can be also equalized. The SWs interact with a rotationally symmetric, anisotropic MTS printed on top of a grounded slab. Modulating the MTS impedance with a period that matches the SW wavelength and employing as the excitation a circular waveguide, field leakage at broadside is obtained with individual control of the two polarizations. Namely, properly adjusting the phase shift between the two orthogonal TE_{11} modes of the circular waveguide, implies RHCP or LHCP with single MTS.

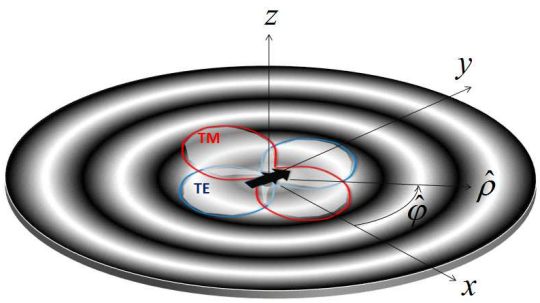

Fig. 1 Pictorial representation of the modulated rotationally symmetric reactance with magnetic dipole excitation. The red and blue lines indicate the amplitude pattern of the SW modes launched on the average impedance surface by a magnetic dipole oriented along y, the latter represented by a double black arrow.

Boundary conditions at the observation point $\boldsymbol{\rho}$ on the MTS are described by an anisotropic, lossless surface impedance tensor, which links the tangential electric ($\mathbf{E}_t$) and the tangential magnetic ($\mathbf{H}_t$) fields at the upper MTS-air interface [10]-[14]

$$\mathbf{E}_t\big|_{0^+} = j\underline{\underline{\mathbf{X}}}\cdot\,\hat{\mathbf{z}}\times\mathbf{H}_t\big|_{0^+} \tag{1}$$

$$\underline{\underline{\mathbf{X}}}(\boldsymbol{\rho}) = \hat{\boldsymbol{\rho}}\hat{\boldsymbol{\rho}}X_{\rho\rho} + \hat{\boldsymbol{\varphi}}\hat{\boldsymbol{\varphi}}X_{\varphi\varphi};\ \langle\underline{\underline{\mathbf{X}}}\rangle = \hat{\boldsymbol{\rho}}\hat{\boldsymbol{\rho}}X_{TM} + \hat{\boldsymbol{\varphi}}\hat{\boldsymbol{\varphi}}X_{TE} \tag{2}$$

where $\hat{\mathbf{z}}$ is the normal to the interface, $\hat{\boldsymbol{\rho}},\hat{\boldsymbol{\varphi}}$ are the unit vectors of the cylindrical coordinate system, and $\langle\cdot\rangle$ represents the space average operator over the circular surface of radius r where the reactance tensor $\underline{\underline{\mathbf{X}}}$ is defined. $\underline{\underline{\mathbf{X}}}$ has principal axes along $\hat{\boldsymbol{\rho}},\hat{\boldsymbol{\varphi}}$ and average eigenvalues defined by the values X_{TM}, X_{TE}. The entries of $\underline{\underline{\mathbf{X}}}$ are modulated by an azimuthally symmetric sinusoidal radial function (see Fig. 1), with modulation index and radial periodicity not yet specified.

In the following, we establish the features of $\langle\underline{\underline{\mathbf{X}}}\rangle$ which provide the phase balancing of the two modes, while the details of the modulation will be discussed in Section III.

A. Phase Matching between TE and TM modes

The practical possibility of implementing a boundary condition described by a diagonal tensor like in (2) is ensured by the fact that any lossless MTS is represented by a Hermitian reactance tensor [10]. Due to this property, $\underline{\underline{\mathbf{X}}}$ always possesses two orthogonal principal axes, that in our case are chosen to be aligned, at any position $\boldsymbol{\rho}$, along the unit vectors of the cylindrical coordinate system. Additionally, $\underline{\underline{\mathbf{X}}}$ depends on both frequency and wavenumber.

Applying the transverse resonance condition [10]-[14], the average eigenvalues $X_{TM,TE}$ are related to the magnitude of the radial propagation wavevector $\mathbf{k}_{TM,TE} = \beta_{TM,TE}\hat{\mathbf{k}}_\rho$ of the SWs launched by a point source located at the origin. These relations are

$$\beta_{TM} = k\sqrt{1+\eta_{TM}^{\,2}};\quad \eta_{TM} = X_{TM}/\zeta \tag{3}$$

$$\beta_{TE} = k\sqrt{1+(1/\eta_{TE})^2};\quad \eta_{TE} = X_{TE}/\zeta \tag{4}$$

where k and ζ are the free-space wavenumber and impedance, respectively. $\eta_{TM,TE}$ are the normalized average reactances, positive (inductive) for the TM_z mode and negative (capacitive) for the TE_z mode.

The key feature to design the antenna is that the two modes are phase-matched, namely, they propagate with the same phase velocity. From (3)-(4), this is ensured by the *phase matching condition*

$$\beta_{TM} = \beta_{TE} = \beta \quad \Rightarrow \eta_{TM}\eta_{TE} = -1 \tag{5a}$$

$$\eta_{TM} = \sqrt{\beta^2/k^2 - 1}\ ;\quad \eta_{TE} = -1/\sqrt{\beta^2/k^2 - 1} \tag{5b}$$

In practice, this condition can be satisfied by using sub-wavelength anisotropic patch elements which allows for independent control of the two reactances $\eta_{TM,TE}$, guarantying, besides, decoupling of the modes.

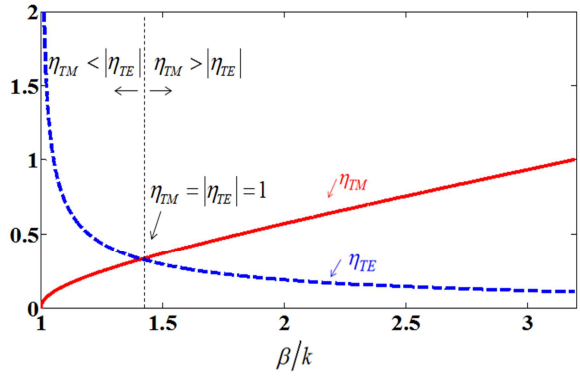

Fig.2. Normalized modal reactances as a function of the normalized propagation constant under phase-matching condition, $\eta_{TM}\eta_{TE} = -1$

We note that the condition in (5) is the same as the one found in [15] for *reflection* properties of a MTS. The latter is used to simulate the effect of a MTS on the internal walls of a horn. Particular cases of these balanced conditions are the so-called *soft* and *hard* conditions introduced by Kildal in the 1980s [16].

Under the assumption (5), and neglecting modal coupling effects, the driving tangential field supported by the MTS is given by

$$\mathbf{E}_{TM} = \hat{\boldsymbol{\rho}} E_{TM} = -jX_{\rho\rho} H_{TM} \hat{\boldsymbol{\rho}} \tag{6}$$

$$\mathbf{E}_{TE} = \hat{\boldsymbol{\varphi}} E_{TE} = jX_{\varphi\varphi} H_{TE} \hat{\boldsymbol{\varphi}} \tag{7}$$

where the two components propagate with the same phase progression. Thereby, the total tangential field in the structure under balanced conditions is given by

$$\mathbf{E}_{tot} = \mathbf{E}_{TM} + \mathbf{E}_{TE} = -jX_{\rho\rho} H_{TM} \hat{\boldsymbol{\rho}} + jX_{\varphi\varphi} H_{TE} \hat{\boldsymbol{\varphi}} \tag{8}$$

B. Polarization Balancing

Let us consider an anisotropic modulated MTS characterized by an average reactance tensor satisfying (5). Let us also assume that the MTS is fed at the center by two infinitesimal horizontal magnetic dipoles with equal momentum, situated over the metallic ground and oriented along $\hat{\mathbf{x}}$ and $\hat{\mathbf{y}}$, respectively (Fig.3).

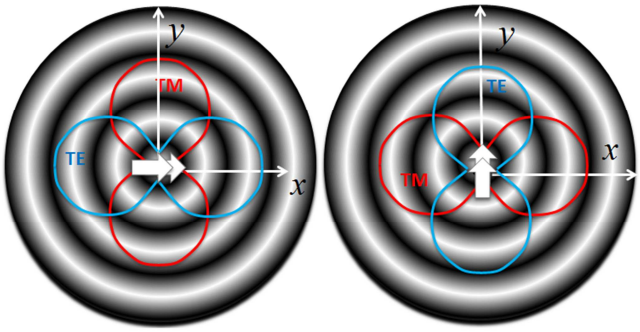

a) b)

Fig. 3 Excitation of the MTS with an infinitesimal horizontal magnetic dipole over the ground plane oriented along a) $\hat{\mathbf{x}}$ and b) $\hat{\mathbf{y}}$.

Denoting by $\mathbf{E}_{tot}^{(x)}$ and $\mathbf{E}_{tot}^{(y)}$ the total tangential fields relevant to the dipoles oriented along *x* and *y*, respectively, one has:

$$\mathbf{E}_{tot}^{(y)} = \mathbf{E}_{TM}^{(y)} + \mathbf{E}_{TE}^{(y)} = -E_{TM}^{(y)} \cos\varphi \hat{\boldsymbol{\rho}} + E_{TE}^{(y)} \sin\varphi \hat{\boldsymbol{\varphi}} \tag{9}$$

$$\mathbf{E}_{tot}^{(x)} = \mathbf{E}_{TM}^{(x)} + \mathbf{E}_{TE}^{(x)} = E_{TM}^{(x)} \sin\varphi \hat{\boldsymbol{\rho}} + E_{TE}^{(x)} \cos\varphi \hat{\boldsymbol{\varphi}} \tag{10}$$

Taking into account that the MTS is perfectly symmetric in azimuth, $E_{TM}^{(x)} = E_{TM}^{(y)} = E_{TM}$ and $E_{TE}^{(x)} = E_{TE}^{(y)} = E_{TE}$. Therefore, polarization balancing is expressed as

$$E_{TM} = E_{TE} \equiv E_0. \tag{11}$$

As a matter of fact, using this latter relationship, (9) and (10) simplify to:

$$\mathbf{E}_{tot}^{(y)} = E_0 \left(-\cos\varphi \hat{\boldsymbol{\rho}} + \sin\varphi \hat{\boldsymbol{\varphi}}\right) = -E_0 \hat{\mathbf{x}} \tag{12}$$

$$\mathbf{E}_{tot}^{(x)} = E_0 \left(\sin\varphi \hat{\boldsymbol{\rho}} + \cos\varphi \hat{\boldsymbol{\varphi}}\right) = E_0 \hat{\mathbf{y}} \tag{13}$$

Introduction of a $\pm 90^\circ$ phase shift between the two excitations, leads to the circularly polarized field:

$$\mathbf{E}_{tot} = \mathbf{E}_{tot}^{(y)} \pm j\mathbf{E}_{tot}^{(x)} = E_0 \left(\hat{\mathbf{x}} \pm j\hat{\mathbf{y}}\right). \tag{14}$$

It is important to observe that while phase-matching is ensured by the condition in (5), which only depends on the MTS properties, the polarization condition in (11) also involves the characteristics of the feed. A discussion on this topic is provided in Sect IV.

III. Design of the Sinusoidal Modulation

Once the characteristics of the average MTS are specified by the phase-matching condition (5), the modulation is set by an azimuthally symmetric sinusoidal radial function, in such a way to get a broadside radiation by a leaky-wave effect [17], and it is given by [3]-[7]

$$X_{\rho\rho} = \zeta \eta_{TM} \left[1 + m_{TM} \cos(2\pi\rho / d_{TM})\right] \tag{15}$$

$$X_{\varphi\varphi} = \zeta \eta_{TE} \left[1 + m_{TE} \cos(2\pi\rho / d_{TE})\right] \tag{16}$$

The main parameters to be controlled are the average normalized reactances $\eta_{TM,TE}$, the modulation indexes $m_{TM,TE}$ (here assumed to be constant), and the periodicities $d_{TM,TE}$ of the sinusoidal radial modulations.

Sinusoidal modulation of the surface reactance generates a complex perturbation $\Delta\beta_{TM,TE} - j\alpha_{TM,TE}$ to the wavenumber $\beta_{TM,TE}$ associated with the average reactance, *i.e.*,

$$\beta_{TM,TE} \to k_{TM,TE}^{(0)} = \beta_{TM,TE} + \Delta\beta_{TM,TE} - j\alpha_{TM,TE} \tag{17}$$

The real part of the perturbation, $\Delta\beta_{TM,TE}$, describes the phase shift suffered by the wavenumber of the SW associated with the average reactance, while the imaginary part, $\alpha_{TM,TE}$, is the leaky attenuation constant introduced by the -1 mode radiation. These perturbations depend mainly on $m_{TM,TE}$ and $\eta_{TM,TE}$, and can be estimated by analyzing the rectilinear problem that locally approximates the radial modulation. The Oliner-Hessel method [17] has been generalized by means of the Green's function of the grounded dielectric slab (extended in the Appendix).

Fig. 4 shows the normalized-to-*k* values of $\Delta\beta_{TM,TE}$ and $\alpha_{TM,TE}$ for different modulation indexes $m_{TM,TE}$ and

normalized average reactance values $|\eta_{TM,TE}|$. As it is shown, $\Delta\beta_{TM,TE}$ and $\alpha_{TM,TE}$ increase with $m_{TE,TM}$, but the impact of the modulation indexes is different for the TE and TM case.

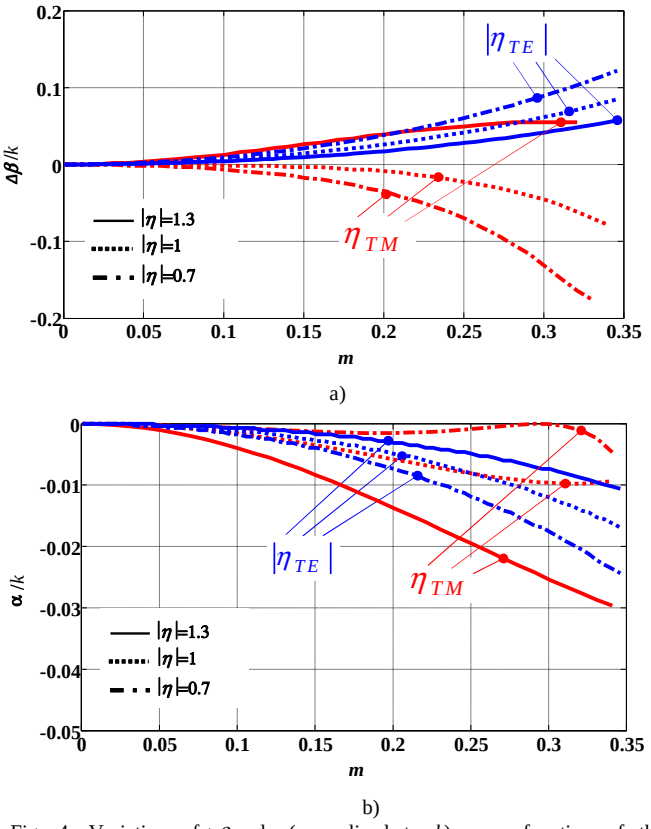

Fig. 4. Variation of $\Delta\beta$ and α (normalized to k) as a function of the modulation index m for three values of the normalized average reactance η, for TM_z(red lines) and TE_z(blue lines).

A. Design of the periodicity

The choice of the periodicity is strictly related to the –1-indexed modes of the Floquet expansion of the TE/TM field. The wavenumbers of these modes are defined as

$$k_{TX}^{(-1)} = \beta + \Delta\beta_{TX} - j\alpha_{TX} - 2\pi / d_{TX} \qquad TX = TE,TM \tag{18}$$

where $\beta = \beta_{TM} = \beta_{TE}$. The -1 indexed field should be the only contribution to the far field radiation. Therefore, (18) should be complemented by the requirement that none of the modes with index different from –1 radiate, namely that their wavenumbers are larger than the free space wavenumber k

$$\left|\mathrm{Re}\left\{k_{TX}^{(n)}\right\}\right| = \left|\beta + \Delta\beta_{TX} + 2\pi n / d_{TX}\right| > k \quad n \neq -1. \tag{19}$$

Broadside radiation of -1 indexed mode implies vanishing of the real part of wavenumber in (18), which leads to

$$d_{TX} = 2\pi / \left(\beta + \Delta\beta_{TX}\right) \qquad TX = TE,TM. \tag{20}$$

identified as *broadside radiation condition*. This means matching the period of the modulation to the wavelength of the TE and TM SWs excited on the average surface, accounting for the polarization-dependent small correction $\Delta\beta_{TM,TE}$. This correction is important for large antennas, since small phase shift can cumulate over the surface.

B. Design of the modulation indexes $m_{TM,TE}$

In order to equalize the amplitude of the two orthogonal components of aperture field all over the aperture, one should impose

$$\alpha_{TM}(\eta_{TM}, m_{TM}) = \alpha_{TE}(\eta_{TE}, m_{TE}) \tag{21}$$

where $\eta_{TE,TM}$ are defined through (5b). This condition is referred to as *amplitude-matching condition* and it is *necessary* for ensuring the CP. We note that since the phase matching condition implies different values of average impedance for TE or TM modes and taking into account that the impact of the modulation indexes is different for each of them, different modulation indexes for TE and TM are required to ensure $\alpha_{TM} = \alpha_{TE}$, *i.e.*, polarization balancing all over the surface. However, this condition is not *sufficient*, since it should be complemented by the feed-balancing condition discussed in Section IV.

IV. Feed Balancing

It has been shown in section II.B that circular polarization is obtained by the TM/TE mode amplitude equalization in (11). Practical conditions on the feed can be found by matching the amplitude of the TM/TE Green's function for a magnetic dipole on the ground plane of a grounded slab with an average sheet reactance on the upper interface. Let us indicate this reactance as $jX_{TX}^{(S)}$ $(TX = TE,TM)$. By using the transmission line network formalism (Fig. 5), it can be assumed that the TM/TE longitudinal (along z) components of the wavenumbers in the dielectric and in air are equalized by the balancing condition; namely, we have

$$k_{z0} = -j\sqrt{\beta^2 - k^2}\ , \ k_{z1} = \sqrt{k_1^2 - \beta^2} \tag{22}$$

for both polarizations. Solving the circuit for the voltage v_2 at the interface (which represents the electric field) it is found

$$v_{2TX} = \frac{v_{TX}\, 2\exp(-jk_{z1}h)}{1 + \exp(-j2k_{z1}h) + \left(\dfrac{Z_{TX1}(Z_{TX}^{(S)} + Z_{TX})}{Z_{TX}^{(S)} Z_{TX}}\right)\left(1 - \exp(-j2k_{z1}h)\right)} \tag{23}$$

where $Z_{TM} = \zeta k_{z0} / k$, $Z_{TE} = \zeta k / k_{z0}$, $Z_{TM1} = \zeta_1 k_{z1} / k_1$, $Z_{TE1} = \zeta_1 k_1 / k_{z1}$, $k_1 = \sqrt{\varepsilon_r}\, k$. The conditions for amplitude matching in (11) becomes $v_{2TM} / v_{TM} = v_{2TE} / v_{TE}$, from which it can be obtained:

$$\frac{v_{TE}}{v_{TM}} = \frac{j\,\mathrm{cosec}(2k_{z1}h)\cot(2k_{z1}h) - \left(\frac{Z_{TE1}(Z_{TE}^{(S)}+Z_{TE})}{Z_{TE}^{(S)}Z_{TE}}\right)}{j\,\mathrm{cosec}(2k_{z1}h)\cot(2k_{z1}h) - \left(\frac{Z_{TM1}(Z_{TM}^{(S)}+Z_{TM})}{Z_{TM}^{(S)}Z_{TM}}\right)} = g(\beta) \quad (24)$$

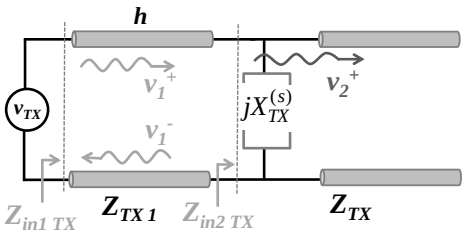

Fig. 5 TM/TE transmission line model of the structure.

When the excitations are given by simple magnetic dipoles (in practice electrically small slots in the ground plane) the ratio in (24) directly provides the relation needed between the magnetic dipole moments. In general, when the structure is excited by an aperture on a ground plane, (24) is applied to the TE and TM components of the Fourier spectrum of the aperture field, evaluated at $k_\rho = \sqrt{k_x^2 + k_y^2} = \beta$. If the feeding is realized by an open ended circular waveguide of radius a excited by a TE_{11} mode, its electric field spectrum $\mathbf{E}_t(\mathbf{k}_t, a)$ (where $\mathbf{k}_t$ denotes the couple of spectral variable k_x, k_y) possesses a closed form $\mathbf{F}(\mathbf{k}_t, a)$ [18]. In such a case, (24) becomes

$$\frac{\mathbf{F}(\mathbf{k}_t, a)\cdot\left(\hat{\mathbf{z}}\times\hat{\mathbf{k}}_\rho\right)}{\mathbf{F}(\mathbf{k}_t, a)\cdot\hat{\mathbf{k}}_\rho} = g(\beta) \quad (25)$$

It can be seen that the left hand side only depends on $k_\rho = \sqrt{\mathbf{k}_t\cdot\mathbf{k}_t} = \sqrt{k_x^2 + k_y^2} = \beta$. Equation (25) establishes, at each frequency, the optimal radius of the circular waveguide a which guarantees perfect amplitude balancing of the two excited TM and TE modes (continuous line in Fig. 6).

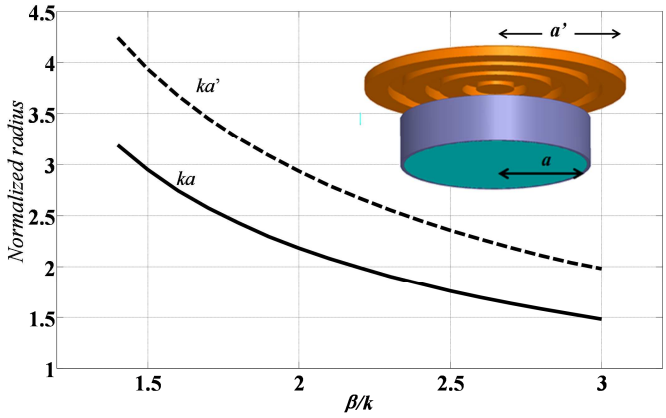

Fig. 6 Optimum radius which guarantees perfect amplitude balance of the excited SWs vs normalized SW wavenumber. Continuous line: direct radiating open ended waveguide fed by a TE_{11} mode (ka). Dashed line: corrugated hat (ka') placed on top of the open ended waveguide.

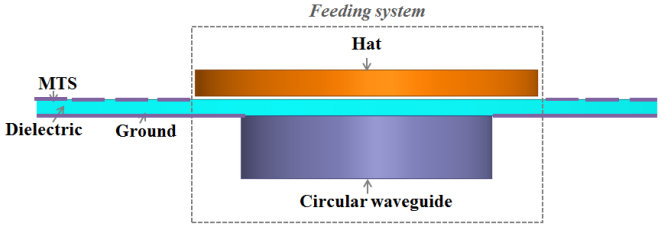

Fig. 7 Details of the employed feeding system.

However, as will be discussed later, TE_{11} mode aperture has proven to be inefficient from the SW excitation point of view, since the space-wave radiation affects considerably the radiation pattern (see Fig. 8c). Due to this fact, it is necessary to introduce a corrugated hat on top of the waveguide, which prevents flowing of the currents on the top of the metal and consequently drastically reduces space-wave contribution. Thus, incorporation of the hat enhances the coupling efficiency from the TE_{11} mode of the circular waveguide to the SWs in the MTS.

The dimension of the outer radius of the corrugated hat is a bit larger than the dimension of the open ended waveguide and it can be controlled in order to balance the TE/TM coupling. The global feeding system can be described invoking a model used for patch antennas: based on the fringe field an equivalent magnetic current ring can be defined, with radius equal to the one of the corrugated disk and effective width equal to the thickness of the substrate. In order to find the new balance conditions, an appropriate modification of the equation (25) should be employed, which involves the derivative of the electric field at the rim of the waveguide:

$$\frac{\frac{\partial\mathbf{F}(\mathbf{k}_t, a')}{\partial a'}\cdot\left(\hat{\mathbf{z}}\times\hat{\mathbf{k}}_\rho\right)}{\frac{\partial\mathbf{F}(\mathbf{k}_t, a')}{\partial a'}\cdot\hat{\mathbf{k}}_\rho} = g(\beta) \quad (26)$$

The hat radius a' which satisfies (26) is represented in Fig. 6 by dashed line.

An orthomode transducer (OMT) can be employed to excite two mutually orthogonal TE_{11} modes in the circular waveguide in phase-quadrature, thus, obtaining the circular polarization as in (14).

V. Overall Antenna Design

A. Continuous MTS

Based on the previous theoretical considerations, a dual-pol MTS antenna has been designed working at 13.5GHz ($\lambda_0 = 22.2mm$). As a preliminary analysis, the MTS has been modeled by means of a penetrable [5]-[7] anisotropic ideal continuous impedance sheet placed on top of a grounded dielectric slab with $\varepsilon_r = 10.2$ and thickness $h = 1.27mm$ (ARLON1000). The antenna has been analyzed using the ANSYS HFSS commercial simulator. The modulation parameters of the impenetrable TM/TE impedance are described in Table I.

TABLE I

	η	m	d/λ_0
TM_z	1.31	0.18	0.61
TE_z	-0.76	0.34	0.58

The modulation is produced by pixelating the continuous boundary condition with square unit cells of size $u = \lambda_0/7$. The radius of the complete structure is $r = 8\lambda_0$.

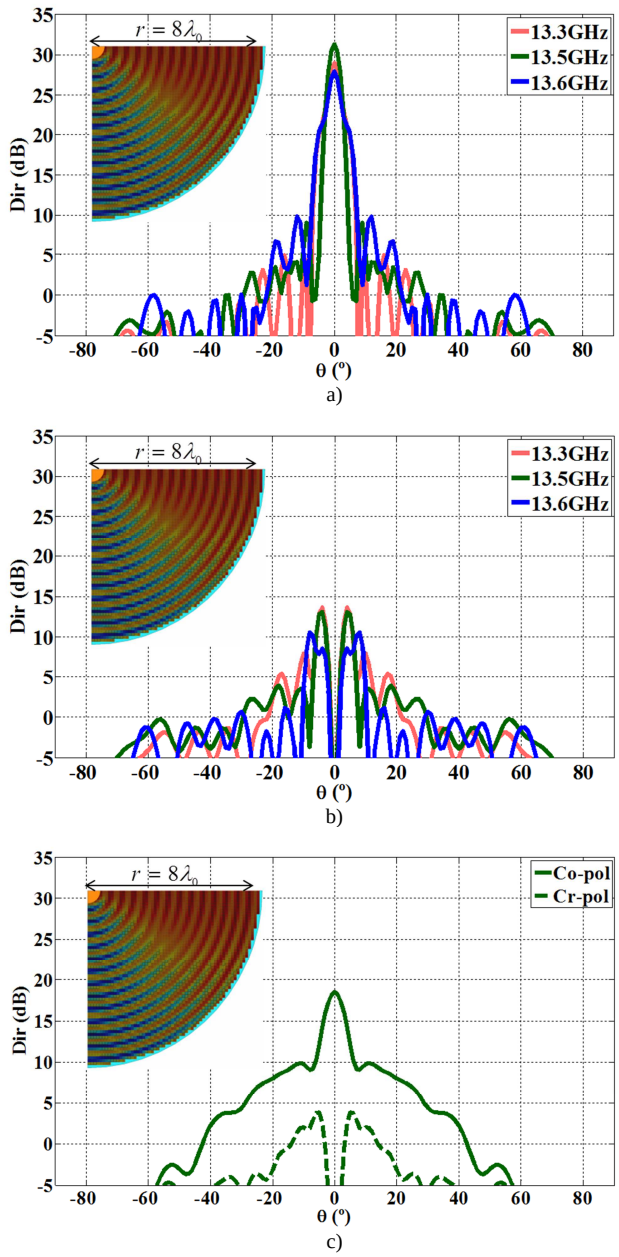

Fig. 8 Simulated co-pol(a) and cross-pol(b) radiation patterns in the $\varphi = 45^o$ cut obtained with the ideal MTS at 13.3GHz(red), 13.5GHz(green) and 13.6GHz(blue). (c) co-pol(continuous) and cross-pol(dashed) radiation pattern on the same antenna obtained by radiation of the open ended circular waveguide without corrugation hat at 13.5GHz.

Based on the feed balancing condition detailed in Section IV, the feed is designed like the one in Fig. 7, with the radius of the circular waveguide equal to $a = 9.6mm$ and the outer radius of the corrugated hat on top equal to $a' = 12.8mm$. Due to the circular symmetry of type "body of revolution 1" [19] (BoR1, namely excited with an azimuthal sine or cosine function), the circular co-pol and cross-pol patterns are obtained by the linear co-pol and cross-pol cut at $\varphi = 45^o$. Fig. 8 shows co-polar (a) and cross-polar (b) components at 13.3GHz, 13.5GHz and 13.6GHz. At 13.5GHz (green line), a maximum directivity of 31.28dB is obtained, with cross-polar component 18dB below the co-polar. The corresponding aperture efficiency is about 50% at the central frequency. For completeness, the radiation pattern at 13.5 GHZ in absence of corrugated top cover is given in the Fig. 8c, where the large cupol-type pedestal added to the main beam is due to the waveguide direct radiation. This effect reduces significantly the antenna gain since the space radiation subtracts power to the main lobe. This is the reason why it is necessary to introduce to corrugated hat.

B. Geometry of the printed elements

The ideal MTS described in the previous section has been implemented by using subwavelength printed elements ("pixels") able to control the polarization performance. When the surface impedance properties of the required non-uniform metasurface vary smoothly, the wavenumber and the local average impedance can be retrieved from the periodic structure that best fits the required local modulated surface impedance value [1],[9]-[14]. TM and TE modes wavenumbers have been obtained using the HFSS eigensolver with periodic boundary conditions in the four vertical walls of the unitary cell, and the corresponding surface impedance has been calculated by (3)-(4).

Several patch geometries have been studied, taking into account the following features:

- The employed pixels have to be anisotropic: the geometry must allow for independent control of the TM and TE contributions.
- The dispersion curves for TM and TE modes should be close to each other around the working frequency to enable the phase-matching condition defined in (5).
- The pixel-elements have to be small enough in terms of wavelength and their axes must be aligned with the wave vector to avoid coupling between modes and consequent introduction of cross-diagonal terms in the reactance tensor.

Elliptical subwavelength elements with an asymmetric cross-shaped aperture inside comply with the previous requirements. In particular, the unitary cell selected for implementing the MTS is presented in Fig. 9.

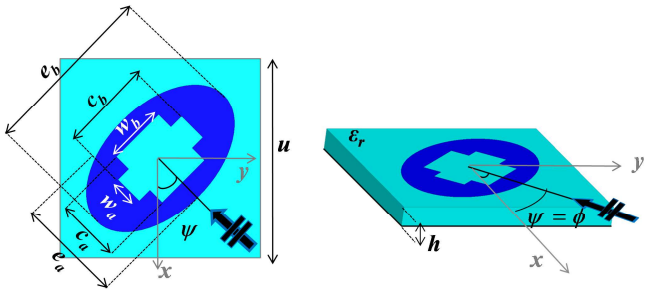

a) b)

Fig. 9 Unitary cell geometry. a) Top view: Details of the elliptical metallic element used for the MTS synthesization, ψ denotes its rotation angle inside the unit cell. b) 3D view, double arrow indicates SW incidence along ϕ.

The geometry has different parameters to play with. The geometrical parameters used in the design are: ellipse size normalized to the unitary cell dimension (e_b/u), ratio between the ellipse axes (e_a/e_b), and normalized dimensions of the asymmetric cross aperture (c_a/e_a), (c_b/e_b), (w_a/u), (w_b/u). Several parametric dispersion analyses have been performed to characterize their effect on TM_z and TE_z SW propagation. The element rotation inside the unit cell (ψ) has been set according to the SW propagation angle ϕ.

As an example, Fig. 10 presents the dispersion curves in the case of the most representative pixels with unit cell dimension $u = \lambda_0/7$ at the operating frequency (13.5GHz). Employed grounded dielectric slab is ARLON1000 with $\varepsilon_r = 10.2$ and thickness h=1.27 mm.

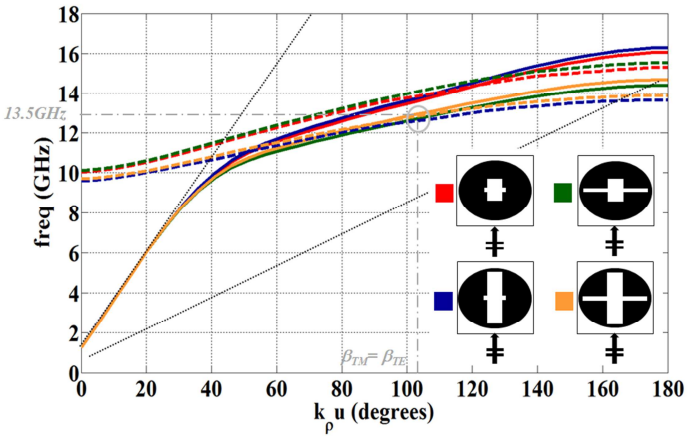

(a)

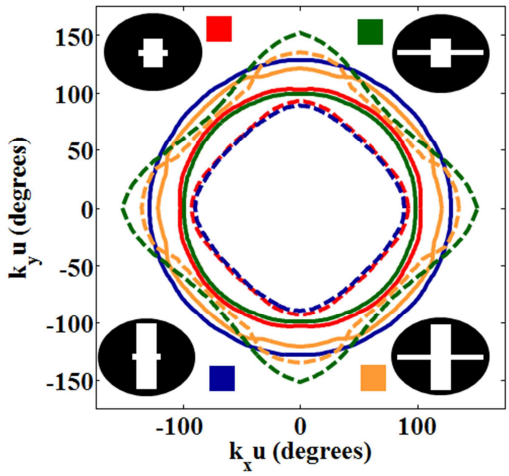

(b)

Fig. 10 TM(continuous lines) and TE(dashed lines) dispersion curves as a function of frequency when $\phi = \psi = 0^\circ$ (a) and isofrequency dispersion curves at 13.5GHz when $\phi = \psi$ (b), for 4 different pixels with the following parameters: $(e_b/u) = 0.9$, $(e_a/e_b) = 0.85$, $(w_a/u) = 0.15$, $(w_b/u) = 0.3$; $(c_a/e_a, c_b/e_b)$ are $(0.6, 0.6)$ red lines; $(0.6, 0.9)$, green lines; $(0.85, 0.6)$, blue lines; $(0.85, 0.9)$, orange lines.

As shown in Fig. 10a, for the $\phi = \psi = 0^\circ$ case, the curves associated with TM and TE SWs dispersion cross at the working frequency ($\beta_{TM} = \beta_{TE}$ at 13.5GHz), ensuring the desired phase matching condition in (5). The geometrical variations of (e_b/u) and (c_b/e_b) mostly affect the TM_z mode. On the other hand, (c_a/e_a) and (w_b/u) affect mainly the TE wavenumber. It has to be also mentioned that the frequency dispersion is more significant for the TE mode, which works closer to its resonance. Fig. 10b shows the spatial dispersion characteristics of both TE and TM SWs for different impinging angles (ϕ) at 13.5GHz, for the same pixel geometry dimensions as in Fig 10a and setting the rotation of the pixel aligned with each SW incidence angle $(\psi = \phi)$. It is clear that the TE curve is much more spatially dispersive than the TM curve.

A data base of several geometrical parameterizations and ϕ values has been obtained. Information corresponding to each analyzed ϕ direction will be later employed to implement the required surface impedance values corresponding to each (ρ_i, φ_i) position of the complete discretized MTS structure.

Fig. 11 and Fig. 12 show X_{TM} and X_{TE} values calculated based on (3)-(4) [1] at 13.5GHz for different pixel shapes when $\phi = \psi = 0^\circ$. Higher values of (c_b/e_b) are associated with higher TM reactance levels. A similar trend is found when the pixel-element is larger inside the same cell (i.e., for increasing e_b/u). On the other hand, higher values of (e_a/e_b), (c_a/e_a) and (w_b/u) increase considerably the TE reactance.

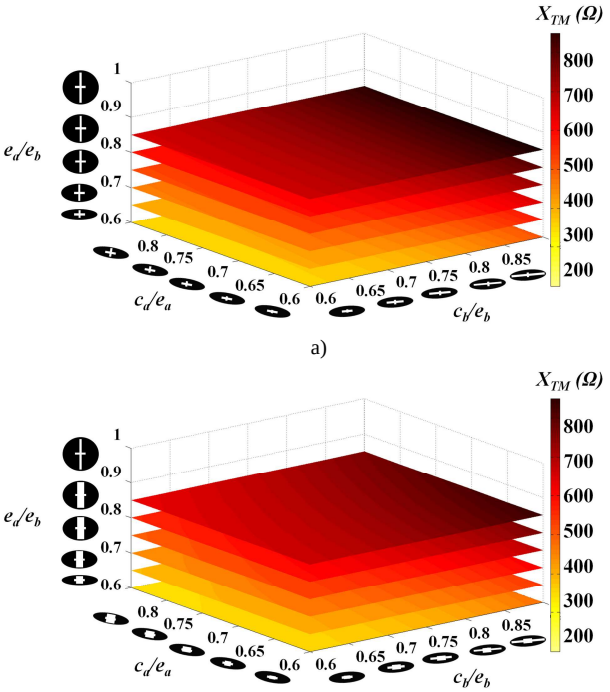

a)

b)

Fig. 11 Impedance maps for TM_z mode obtained at 13.5GHz for different pixel shapes when $\phi=\psi=0°$. a) $(w_b/u)=0.15$. b) $(w_b/u)=0.3$.

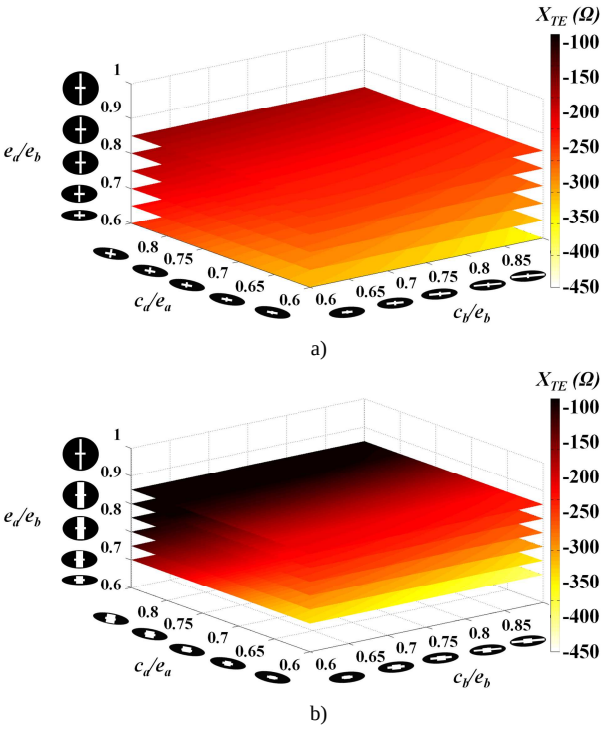

a)

b)

Fig. 12 Impedance maps for TE_z mode obtained at 13.5GHz for different pixel shapes when $\phi=\psi=0°$. a) $(w_b/u)=0.15$. b) $(w_b/u)=0.3$.

C. Full wave analysis of the antenna.

The design of the MTS has been carried out by means of the pixels described in the previous section. The modulation of the surface impedance has been designed following the ideal MTS reactance detailed in Section V.A. The radius of the circular antenna is $r=8\lambda_0$ ($\lambda_0=22.2mm$) and the feeding system is the one described in Section IV. Details of the implemented model can be seen in Fig. 13.

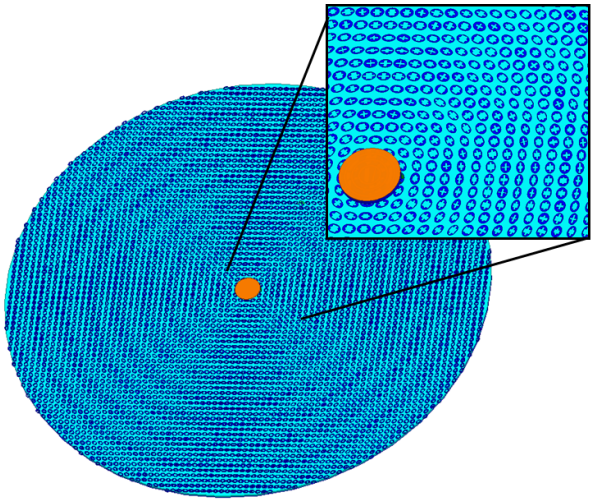

Fig. 13 Top view of the complete MTS antenna implemented with elliptical pixels with a cross-shaped aperture inside and zoom of the center.

A proper selection of the pixel geometries at each (ρ_i,φ_i) position of the antenna provides the sinusoidally modulated surface impedance characteristics required for each TM and TE propagating mode.

As in the previous section with the ideal MTS, one quarter of the structure with pixels has been simulated employing symmetries. Fig.14 shows the $\varphi=45^o$ cut of co-polar and cross-polar components (corresponding to the RHCP and LHCP components) of the radiated field at 13.3GHz, 13.4GHz and 13.5GHz. At 13.4GHz, a maximum directivity of 27.3dB is obtained with cross-polar component 21dB below the co-polar level. It can be concluded that the employed feeding system and implemented MTS balance correctly the amplitudes of the propagating modes and guarantee their contribution to the boresight with circular polarization. Nevertheless, there is a loss of gain of 4dBi with respect to the ideal continuous impedance model, and consequently the aperture efficiency is about 20%. The main reason for the decrease in the aperture efficiency is due to the Cartesian-lattice discretization carried out for adapting the periodic unit cell to the theoretical, circularly symmetric, homogeneous surface impedance. While this discretization is not a problem for the TM case (and therefore not a problem for single CP antennas), it is critical for TE mode. There are two reasons that lead to this assumption: on the one hand, the isofrequency dispersion curves associated with the TE case are quite irregular and more sensitive to the rotation of the geometry into the square lattice (see Fig. 10b); on the other hand, the modulation index required for the TE mode is higher. Therefore, a local compensation is required along both the azimuthal direction (due to TE isofrequency dispersion) and the radial direction (due to high modulation for TE), which has been obtained by adjusting the rotation and the dimension of each pixel inside the lattice. Although these considerations reduce the average discretization error in the TE impedance

synthesis, the adjustments also affect and slightly deteriorate the TM impedance synthesis error, resulting in a reduction of the overall efficiency.

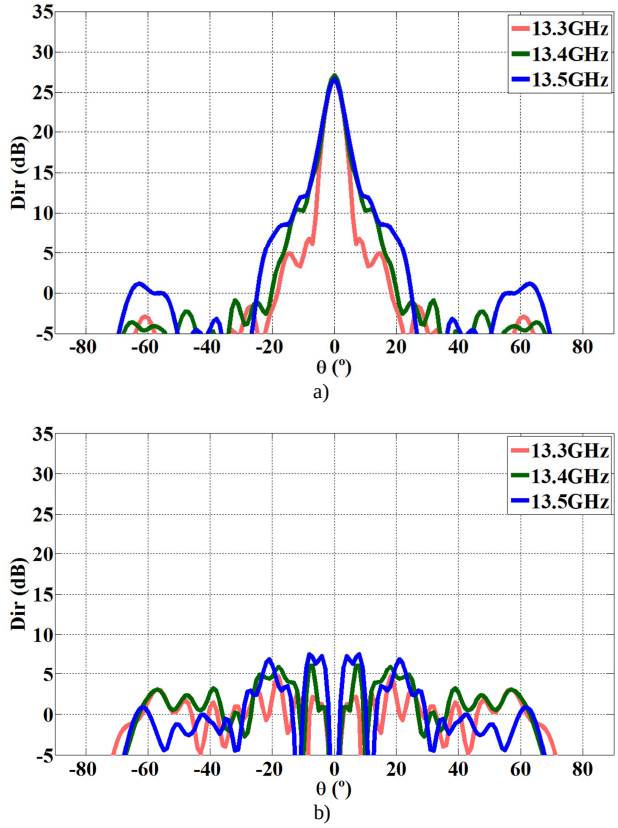

Fig.14 Simulated co-pol(a) and cross-pol(b) radiation patterns in the $\varphi = 45^{o}$ cut obtained with the MTS synthesized with pixels, at 13.3GHz(red), 13.4GHz(green) and 13.5GHz(blue).

Fig.15 shows frequency dependence of the directivity and gain. Gain over 25 dBi is obtained in a 1.5% bandwidth. The corresponding radiation efficiency is about 70%. The main reason for this narrowband response is the frequency dispersion shown by the pixel for the TE mode. Shifting of frequency implies significant cumulative aperture phase error, and consequent reduction of gain, especially for large structures.

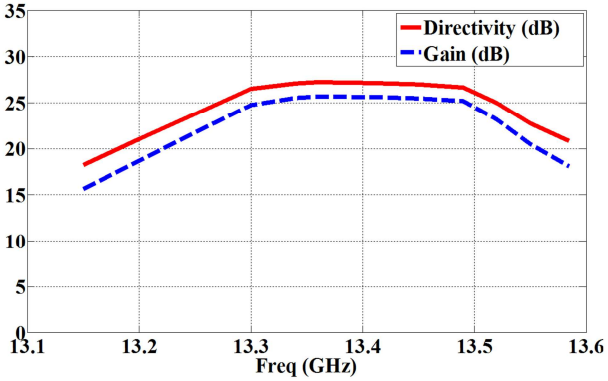

Fig.15 Frequency dependence of directivity and gain.

VI. Conclusion

A MTS Ku-band antenna capable to provide a broadside beam with dual circular polarization has been designed. The capability to obtain dual polarization with the same structure is important in many applications, and it is a challenge for MTS antennas. The presented solution operates on the interaction between the MTS and two cylindrical-wavefront SWs with TM and TE polarization, which propagate in the structure with phase and amplitude matching. Broadside radiation is obtained by a periodic modulation that matches the wavelength of the two SWs simultaneously. Amplitude matching of the excited SWs is guaranteed by the correct design of the feed, which is not purely TM as in other single circular polarization configurations [4]. Appropriate modulation of the MTS impedance corresponding to each mode controls the field radiation. Unbalancing of the leakage parameters α_{TM}, α_{TE} can deteriorate both the azimuthal symmetry of the beam and the cross-polar performance.

Practical implementation of the MTS has been carried out employing a dense texture of anisotropic sub-wavelength elements, consisting of metal elliptical patches with an asymmetric cross-shaped aperture inside, printed on a grounded dielectric slab. Simulation results show -21dB level of cross-pol within a bandwidth of few percent around the working frequency (13.4GHz). Antenna efficiency is about 15.5%. The main reason of the narrowband behavior and efficiency drop is found in the space and frequency dispersive behavior of the TE mode when it propagates in the structure. In fact, the design is much more challenging in comparison to the single polarized MTS structures, due to the fact that two propagating modes with different nature and perfectly synchronized are required to obtain the desired performance.

Appendix

The complex TM-TE LW wavenumber which leads to the plots in (4) has been obtained by solving the dispersion equation of the rectilinear problem that locally approximates the radial modulation. The rectilinear problem is characterized by a sinusoidal homogenised penetrable impedance $Z_S(x) = jX(1+M\cos(2\pi x/d))$ which describes the cladding of the canonical problem. To this end, we set the boundary conditions

$$\mathbf{E}(x,0) = Z_S(x)\mathbf{J}_S(x,0) \tag{27}$$

where $\mathbf{E}$ is the field at the interface and $\mathbf{J}_s$ is the average electric current flowing in the impedance. For both the TE and the TM case, the problem is formulated by expanding the field and the current in terms of Floquet modes (FM) with wavenumbers $k_{xn} = k_x + 2\pi n/d$, $n = 0, \pm 1, \pm 2$. The electric field $\mathbf{E}$ is obtained by weighting each FM component of the current by the pertinent spectral TM/TE Green's function of the grounded slab sampled at k_{xn}. This leads to

$$\sum_n G^{TM/TE}(k_{xn},0) I_n e^{-jk_{xn}x} = \tag{28}$$

$$= X(1+M\cos(2\pi/d))\sum_n I_n e^{-jk_{xn}x}$$

where $G^{TM/TE}$ denote the Green's function of the grounded slab for the TE or TM modes, defined as follows:

$$G^{TM} = -Z_0^{TM}\, jZ_1^{TM}\tan(k_{z1}h)/\left(Z_0^{TM} + jZ_1^{TM}\tan(k_{z1}h)\right) \quad (29)$$

$$G^{TE} = -Z_0^{TE}\, jZ_1^{TE}\tan(k_{z1}h)/\left(Z_0^{TE} + jZ_1^{TE}\tan(k_{z1}h)\right) \quad (30)$$

The numerical solution of (28) in terms of the complex wavenumber k_x (and therefore the propagation and attenuation constants of the leaky-wave) is obtained by reducing (28) in a continuous-fraction determinantal equation following the procedure suggested by Oliner and Hessel in [17].

ACKNOWLEDGMENT

The authors would like to thank Marco Sabbadini from ESA-ESTEC for the useful suggestions. This work was supported by the COST ACTION IC1102, the NEWFOCUS Research Networking Programme, Spanish Ministry of Science and Innovation (project TEC2013-47753-C3-1-R) and by University of Siena and Public University of Navarre.

REFERENCES

[1] B. H. Fong, J. S. Colburn, J. J. Ottusch, J. L. Visher, and D. F. Sievenpiper, "Scalar and tensor holographic artificial impedance surfaces", *IEEE Trans. Antennas Propag.*, vol. 58, no. 10, pp. 3212–3221, Oct. 2010.

[2] A. Patel and A. Grbic, "A printed leaky-wave antenna based on a sinusoidally-modulated reactance surface", *IEEE Trans. Antennas Propag., vol.59*, no.6, pp. 2087-2096, June 2011.

[3] G. Minatti, F. Caminita, M. Casaletti, and S. Maci, "Spiral leaky-wave antennas based on modulated surface impedance", *IEEE Trans. Antennas Propag.*, vol. 59, no. 12, pp. 4436–4444, Dec. 2011.

[4] S. Maci, G. Minatti, M. Casaletti and M. Bosiljevac, "Metasurfing: Addressing Waves on Impenetrable Metasurfaces", *IEEE Antennas and Wireless Propag. Letters*, vol. 10, pp. 1499–1502, Jan. 2011.

[5] M. Faenzi, F. Caminita, E. Martini, P. De Vita, G. Minatti, M. Sabbadini, anf S. Maci, "Realization and Measurement of Broadside Beam Modulated Metasurface Antennas", *IEEE Antenas and Wireless Propag. Letters*, vol. pp, no. 99, pp. 1-1, Dec. 2015.

[6] G. Minatti, S. Maci, P. De Vita, A. Freni, and M. Sabbadini, "A circularly-polarized isoflux antenna based on anisotropic metasurface", *IEEE Trans. Antennas Propag.*, vol. 60, no. 11, pp. 4998–5009, Nov. 2012.

[7] G. Minatti, M. Faenzi, E. Martini, F. Caminita, P. De Vita, D. González-Ovejero, M. Sabbadini, and S. Maci, "Modulated Metasurface Antennas for Space: Synthesis, Analysis and Realizations", *IEEE Trans. Antennas Propag.*, vol. 63, no. 4, pp. 1288–1300, Apr. 2015.

[8] A. Tellechea, E. Martini, D. Gonzalez-Ovejero,M. Faenzi, G. Minatti, S. Maci, "Dual Band IsofluxUltraflat Meta Antennas", presented at *9th European Conference on Antennas and Propagation*, Lisbon, Portugal, Apr. 12-17, 2015.

[9] C. Pfeiffer and A. Grbic, "Planar lens antennas of subwavelength thickness: collimating leaky-waves with metasurfaces", *IEEE Trans. Antennas Propag., vol.*63, no.7, pp. 3248-3253, July 2015.

[10] J. Hoppe and Y. R. Samii, *Impedance Boundary Conditions in electromagnetics*.Washington, DC: Taylor and Francis, 1995, pp. 135–137.

[11] S. Maci, M. Caiazzo, A. Cucini, and M. Casaletti, "A pole-zero matching method for EBG surfaces composed of a dipole FSS printed on a grounded dielectric slab", *IEEE Trans. Antennas Propag.*, vol.53, no. 1, pp. 70–81, Jan. 2005.

[12] A.M. Patel, A. Grbic, "Transformation Electromagnetics Devices Based on Printed-Circuit Tensor Impedance Surfaces," *Microwave* Theory and Techniques, IEEE Transactions on , vol.62, no.5, pp.1102-1111, May 2014.

[13] A. M. Patel, A. Grbic, "Effective surface impedance of a printed circuit tensor impedance surface (PCTIS)," *Microwave Theory and Techniques, IEEE Transactions on*, vol.61, no.4, pp.1403,1413, 2013.

[14] A. M. Patel, A. Grbic, "Modeling and Analysis of Printed-Circuit Tensor Impedance Surfaces," *IEEE Trans on Antennas Propagat,* , vol.61, no.1, pp 211-220, 2013.

[15] E. Lier, D.H. Wemer, C.P. Scarborough, Q. Wu, and J. A. Bossard, "An octave-bandwidth negligible-loss radiofrequency metamaterial ", *Nature Materials*, vol. 10, pp. 216–222, Jan. 2011.

[16] P.-S. Kildal, "Artificially soft and hard surfaces in electromagnetics" , *IEEE Trans. Antennas Propag*., vol. 38, no. 10, pp. 1537–1544, Oct. 1990.

[17] A. Oliner and A. Hessel, "Guided waves on sinusoidally-modulatedreactance surfaces," *IRE Trans. Antennas Propag*., vol. 7, no. 5, pp.201–208, Dec. 1959.VVV

[18] G. Borgiotti, "Modal Analysis of Periodic Planar Phased Arrays of Apertures", *Proc. IEEE*., vol. 56, no. 11, pp. 1881–1892, Nov. 1968.

[19] Per-Simon Kildal, "Rotationally symmetric antennas" in *Foundation of Antenna Engineering*, 1st ed., Gothenburg, Sweden.

Amagoia Tellechea Pereda was born in Betelu, Navarra, Spain, in 1986. She received the Ingeniero de Telecomunicación and Master en Comunicación degrees from the Public University of Navarra, Pamplona, Spain, in 2011 and 2012, respectively. She joined the Antennas Group at the Electrical and Electronic Engineering Department in UPNA where she is currently working under a scholarship towards the Ph.D. degree. Her research interests focus mainly on Electromagnetic Bandgap materials and Metasurfaces for space applications.

Francesco Caminita received the Laurea degree (*cum laude*) in telecommunications engineering and the Ph.D. degree in information engineering from the University of Siena, Italy, in 2005 and 2009, respectively. He is presently a Research Associate at the University of Siena. Since 2006, he has been involved in projects funded by the European Space Agency (ESA) and the European Union (EU) concerning software antenna modeling. Since 2014 he has also been with the start-up Wave Up Srl, Florence, Italy. His research interests include the fields of computational electromagnetics, metamaterial characterization, analysis and design of metasurface antennas. Dr. Caminita was a co-recipient of the Best Paper Award on Antenna Theory at the 5th European.

[20] **Enrica Martini** (S'98-M'02-SM'13) was born in Spilimbergo (PN), Italy, in 1973. In 1998, she received the Laurea degree (cum laude) in telecommunication engineering from the University of Florence, Italy, where she worked under a one-year research grant from the Alenia Aerospazio Company,

Rome, Italy, until 1999. In 2002, she received the PhD degree in informatics and telecommunications from the University of Florence and the Ph.D. degree in electronics from the University of Nice-Sophia Antipolis, under joint supervision.
In 2002, she was appointed Research Associate at the University of Siena, Italy. In 2005, she received the Hans Christian Ørsted Postdoctoral Fellowship from the Technical University of Denmark, Lyngby, Denmark, and she joined the Electromagnetic Systems Section of the Ørsted•DTU Department until 2007. Since 2007 she has been a Postdoctoral Fellow at the University of Siena, Italy. Since 2012 she has also been with the start-up Wave Up Srl, Florence, Italy. Her research interests include metamaterial characterization, metasurfaces, electromagnetic scattering, antenna measurements, finite element methods and tropospheric propagation.

Iñigo Ederra received the Ingeniero de Telecomunicación and Ph.D. degrees from the Universidad Pública de Navarra, Pamplona, Spain, in 1996 and 2004, respectively. In 1997, he joined the Microwave and Millimetre Wave Group, Universidad Pública de Navarra. From 1999 to 2000 he was with the European Space Research and Technology Centre (ESTEC), ESA, Noordwijk, The Netherlands, where he was working on Electromagnetic Bandgap materials and their applications in the field of antennas. Since 2001 he is with the Antenna Group, Universidad Pública de Navarra. From June to October 2002 he was visitor scientist at the Rutherford Appleton Laboratory, Chilton, Didcot, UK, participating in the Startiger project. His research interests are in the field of Electromagnetic Bandgap materials, Metamaterials and Metasurfaces and their applications in microwave, millimetre wave and THz components and antennas.

Juan Carlos Iriarte (Pamplona, Navarra, 1978). PhD. In Telecomunication Engineery, 2008, Universidad Pública de Navarra, Spain
Since July 2001 he is with the Antennas Group at the Electrical and Electronic Engineering Department in UPNa. From September 2002 to March 2004, he was joined thanks to a University grant to the Antennas Group where he was involved in the design of Electromagnetic Band Gap Antennas, while he was doing his Ph. Degree studies. From March 2004 he is a research assistant in the UPNa. His Phd Dissertation was awarded with the 1st ISDEFE award in Security and Defence given by the Spanish COIT (Colegio Oficial Ingenieros Telecomunicacion) in 2010. He has been involved in 45 research projects and company contracts being the IP in 7 of them. He has 14 publications, 2 chapters of books and more than 70 conference papers. List available online: www.antenas.unavarra.es
His current areas of research are in the field THz and millimeter waves imaging and sensing and in metamaterials and metasurfaces for microwave, millimetre and THz wave antenna applications with emphasis on space antenna applications.

Ramón Gonzalo (M'94) was born in Logrono, La Rioja, on July 15, 1972. He received the M.Sc. and the Ph.D. degrees in ingeniero de telecomunicacion, both with honors, from the Public University of Navarra (UPNa), Spain. Since October 1995, he has been with the Antennas Group at the Electrical and Electronic Engineering Department in UPNa, where he currently is Full Professor. From September 1997 to December 1998, he was joined as Research Fellow to the Antenna Section in ESA-ESTEC, where he was involved in the modeling and design of electromagnetic crystal devices at microwave and millimeter-wave frequencies. He has been involved in more than 25 research projects, European and national level, acting as coordinator in several of them. He has more than 60 journal publications in peer review magazines and 100 conference papers related to his research lines. From January 2006 until April 2008, he was acting as sub-director of the Engineering Faculty and from April 2008 to December 2010 as Head of Electrical and Electronic Engineering Department. Dr. Gonzalo was corecipient of the LAPC 2006, LAPC 2007, and IWAT 2007 Best Paper Award. His current area of research is in the field of terahertz technologies, electromagnetic band gap technology, and design of waveguide transmission lines and corrugated horn antennas.

Stefano Maci got his Laurea degrees at University of Florence, in 1987. He is presently Professor at the University of Siena, and Director of the PhD School of Information Engineering and Science, which presently includes about 60 PhD students. His present research interests are focused on high-frequency and beam representation methods, computational electromagnetics, large phased arrays, planar antennas, reflector antennas and feeds, metamaterials and metasurfaces. He was the founder of the European School of Antennas (ESoA). He has been a former member of the AdCom of IEEE Antennas and Propagation Society (AP-S), associate editor of AP-Transaction, Chair of the Award Committee of IEEE AP-S, and member of the Board of Directors of the European Association on Antennas and Propagation (EuRAAP). He has been also a member of the Governing Board of the European Science Foundation Project "NewFocus", a Distinguished Lecturer of the IEEE Antennas and Propagation Society (AP-S), and a member of the Antennas and Propagation Executive Board of the Institution of Engineering and Technology (IET, UK). He has been one of the founder of the consortium FORESEEN on Nanoarchitectronics. Stefano Maci is presently Director of ESoA, director of FORESEEN, a member of the Technical Advisory Board of the URSI Commission B. His research activity is documented in 10 book chapters, 140 papers published in international journals, (among which 90 on IEEE journals), and about 300 papers in proceedings of international conferences. His h-index is 30, with around 4000 citations (source Google Scholar).